Dicle University
Journal of Engineering
https://dergipark.org.tr/tr/pub/dumf
duje.dicle.edu.tr

Research Article

Photovoltaic Fault Detection Using SE-MobileNet: A Lightweight Channel Attention Network

Hasan POLAT[1*], Oğuz Kaan POLAT[2]

[1] Bingöl University, Department of Electrical and Energy, hasanpolat@bingol.edu.tr, Orcid No: 0000-0001-5535-4832
[2] Bingöl University, Department of Renewable Energy Systems, 248241030@bingol.edu.tr, Orcid No 0009-0002-2550-8153

ARTICLE INFO

Article history:

Received 9 April 2026
Received in revised form 11 May 2026
Accepted 18 June 2026
Available online 28 July 2026

Keywords:

Renewable energy, Solar energy, Photovoltaic, PV Fault Detection, Deep Learning, Machine Learning

Doi: 10.24012/dumf.1926748

* Corresponding author

ABSTRACT

The global energy sector is increasingly shifting from fossil-fuel-based generation to renewable energy sources, with solar photovoltaic (PV) systems playing a critical role in sustainable electricity production. However, the operational efficiency of PV panels strongly depends on maintaining their surface cleanliness and structural integrity. Therefore, early and accurate fault detection is essential to ensure maintained efficiency and system reliability. This study introduces a lightweight deep learning framework, termed SE-MobileNet, for diagnosing PV surface faults such as dust, dirt, and bird droppings, as well as physical and electrical damage. The proposed model incorporates a Squeeze-and-Excitation (SE) block into a MobileNet backbone to enable channel-wise feature recalibration without imposing a significant computational burden. Experimental results demonstrate that this adaptive channel-wise refinement yields a notable improvement in classification performance, increasing the macro F1-score from 0.776 to 0.837, while outperforming a range of benchmark convolutional and transformer-based models. Furthermore, the model achieves a favorable trade-off between accuracy and computational complexity, with an inference time of 12.73 ms and 78.54 FPS, supporting near real-time deployment in practical PV monitoring applications.

Introduction

The global energy market is undergoing a transition from traditional fossil fuel–based systems to environmentally friendly, clean, and sustainable energy production systems. Solar energy, as an easily accessible and entirely clean energy source, is leading this transition [1], [2]. Photovoltaic (PV) panels are the primary instrument used to generate electricity from solar energy. They are made of semiconductor materials. When sunlight reaches the PV surface, photons are absorbed by the semiconductor material, generating electron–hole pairs that drive the conversion of solar energy into electrical power [3]. However, maintaining the structural integrity and surface cleanliness of PV panels is crucial for ensuring long-term efficiency and reliable operation. Dust, dirt, and bird droppings, in particular, can significantly reduce electricity generation efficiency, while the failure to detect electrical or physical damage at an early stage may lead to permanent deterioration [4]. Thus, it is essential to implement systematic inspection strategies for PV panels, incorporating early fault detection and timely intervention, to ensure the sustained and optimal operation of both grid-connected and off-grid solar systems.

Manually inspecting PV panels is inherently labor-intensive, time-consuming, and practically infeasible given the large-scale nature of modern installations. To address these limitations, computer-aided detection systems offer an effective and scalable alternative. With recent advances in computer vision, PV panel faults can be accurately identified using imaging methods such as electroluminescence (EL), infrared (IR), and visible spectrum (RGB) imaging data, each providing complementary insights into different types of faults. Also, these approaches enable non-contact, rapid, large-scale and full automated inspection, thereby significantly enhancing both detection accuracy and operational efficiency compared to traditional manual methods [5]. Furthermore, the availability of large-scale PV datasets facilitates the development of more advanced and robust machine learning approaches. In this context, there has been a significant increase in machine learning-based research on PV fault detection, diagnosis, and localization over the past decade [6].

Recent advancements in deep learning have considerably improved the effectiveness of image-based fault detection in photovoltaic panels. More specifically, convolutional neural networks (CNN)s have demonstrated outstanding performance in this domain due to their powerful feature extraction capabilities for image modalities [7]. In contrast to traditional handcrafted feature extraction techniques, CNN-based deep learning models automatically learn hierarchical and highly discriminative features from raw data. Coupled with their end-to-end learning frameworks, this makes deep learning approaches a more robust and reliable solution for complex image analysis task. Although deep learning has demonstrated high accuracy in PV panel fault detection, its substantial model complexity and large-scale data requirements indicate that these architectures still require further improvement. In addition, challenges such as data imbalance, the need for effective data augmentation strategies, and the dependency on robust preprocessing pipelines remain critical issues that can significantly affect model performance and generalization [8]. Therefore, current research trends in PV fault detection and classification emphasize the development of more efficient and robust architectures to address these challenges.

This study proposes a lightweight deep learning framework based on a Squeeze-and-Excitation [9] enriched MobileNet [10] architecture (SE-MobileNet) for PV panel fault detection and classification. The proposed model utilizes a channel-wise attention mechanism to enhance feature representation capabilities, while maintaining low computational complexity through a lightweight backbone design. In contrast to conventional deep learning models that prioritize accuracy at the expense of efficiency, the proposed approach aims to achieve a better trade-off between detection performance and model complexity.

The main contributions of this study can be summarized as follows:

- A lightweight SE-MobileNet architecture is proposed for PV panel fault detection.
- A channel-wise attention block is incorporated to enhance feature representation capability.
- A comprehensive comparison is conducted with other CNNs and Transformer-based models.
- The proposed model is designed to provide a favorable trade-off between accuracy and model complexity.
- The framework is suitable for real-time and large-scale PV monitoring applications.

Related Work

For solar PV systems, early fault detection and accurate classification of fault types are crucial for minimizing power losses, extending the life span, and preventing irreversible damage. Therefore, the researchers have focused on developing reliable and robust fault detection and classification methods for PV systems. The fault detection approaches mostly rely on data obtained from non-electrical imaging modalities and electrical measurements [6], [8]. In particular, non-electrical imaging methods enable large-scale data acquisition using relatively simple setups, thereby facilitating the application of advanced machine learning models. Previous studies on PV fault detection, classification, and localization have explored conventional and deep learning, which are reviewed in this section under separate subheadings.

Conventional Models

Conventional approaches seek to characterize PV module faults by extracting handcrafted features, including filtering-based descriptors, histogram representations, thresholding techniques, and pixel intensity distributions [11]. The extracted features are subsequently fed into classical and relatively simple classifiers for fault detection and diagnosis. For example, Niazi et al. [12] used a Naive Bayes classifier with texture features extracted from thermal images to classify PV panels as defective or non-defective, achieving 98.4% accuracy in binary classification. Et-taleby et al. [13] introduced a hybrid fault detection and classification pipeline integrating thermal image processing and Mamdani fuzzy logic to diagnose six critical PV fault types. Their framework extracts physically interpretable features, including maximum and minimum temperatures, as well as hotspot and shadow ratios. Shaban et al. [14] fused statistical and texture features for the detection and classification of PV panel defects using EL images. The proposed framework adopts a two-stage classification strategy, including both binary and multi-class classification. In the first stage, a Naive Bayes classifier is used to detect abnormal panels, followed by a multi-layer perceptron (MLP) for classifying defective panels into different fault categories. Similarly, Ali et al. [15]also proposed a hybrid feature engineering-based framework for PV fault detection and classification using infrared thermography. A fused feature vector consisting of RGB features, texture descriptors, HOG, and Local Binary Patterns (LBP) was constructed and classified using an SVM model. The proposed approach achieved 92% testing accuracy for a three-class classification task.

Traditional approaches primarily rely on carefully designed handcrafted features. The feature extraction and selection are often dependent on domain expertise and iterative trial-and-error processes, making the pipeline complex and time-consuming. Moreover, classical classifiers tend to provide limited generalization capability when applied to large-scale and complex datasets, which remains a significant limitation.

Deep Learning Models

Deep learning has emerged as a promising pathway across diverse domains, enabling tasks such as visual PV inspection, anomaly detection, targeted defect identification, and simultaneous object recognition [5]. Through their hierarchical architectures, these models automatically learn and refine representations from low-level patterns to high-level semantic information, eliminating the need for manual feature engineering.

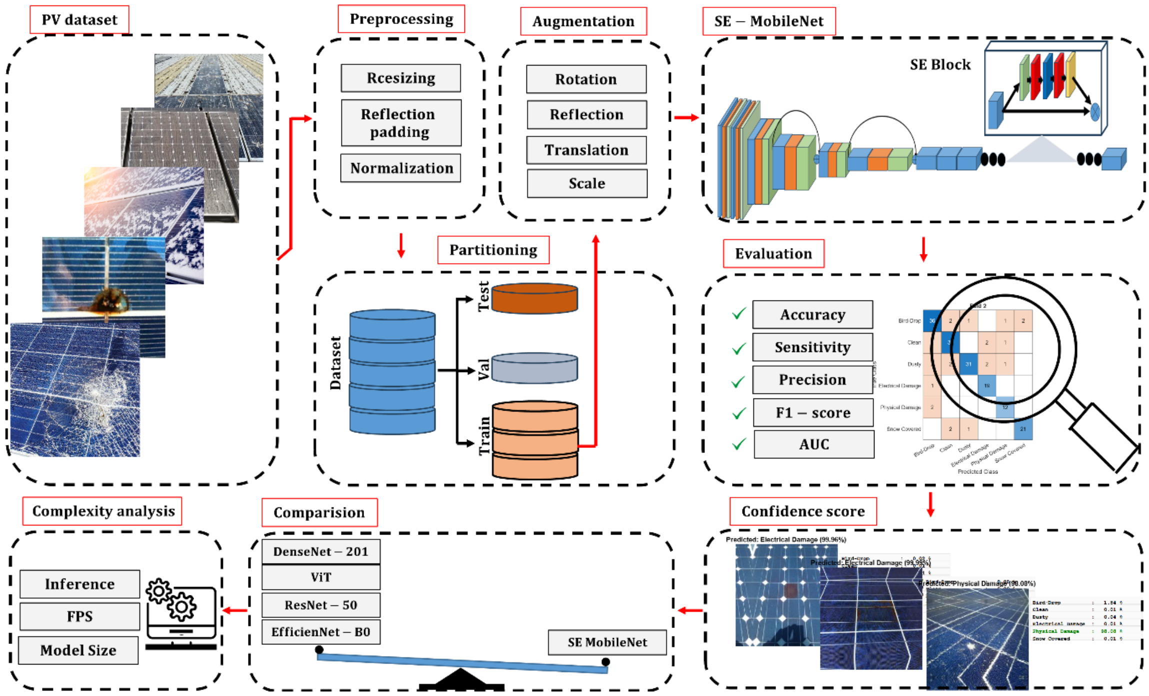

Figure 1. Schematic overview of the proposed PV panel fault detection pipeline

However, the effective training of such architectures relies on large-scale labeled data, the acquisition and annotation of which are both costly and time-consuming [16]. In recent years, the increasing availability of large-scale annotated datasets has significantly accelerated the development of deep learning-based approaches for remote inspection and fault analysis of PV systems. Malek et al. [17] proposed an efficient feature engineering approach based on a pre-trained VGG-16 model for PV fault detection. Features extracted from convolutional and pooling layers were subsequently fed into a random forest (RF) classifier for binary classification and a logistic regression (LR) model for fault categorization, achieving accuracies of 97.54% and 89.44%, respectively. Sonawane et al. [18] investigated various class balancing strategies to address inter-class imbalance in the detection of diverse PV fault types from RGB images using deep learning. They employed an InceptionV3 model and further validated the robustness of the proposed balancing strategy using a YOLOv8 classifier. In another study, Tang et al. [19] proposed a transfer learning-based depth reduction framework (TLDR-CNN) for PV fault classification using infrared imagery. By integrating a multi-scale feature extraction module into a VGG-16 backbone, the proposed model achieved improved classification performance while reducing computational complexity. Similarly, Bamisile et al. [20] introduced an attention-based residual network with a multi-scale convolutional structure for infrared-based PV fault classification. The proposed model achieved 0.968 accuracy and 0.981 ROC-AUC in binary classification, and up to 0.971 accuracy and 0.993 ROC-AUC in multi-class settings, demonstrating strong robustness under class imbalance and real-world thermal variability. Ledmaoui et al. [21] introduced an explainable AI-based framework built upon an enhanced VGG-16 model for anomaly detection in PV panels using RGB imagery. The model effectively identified defects such as dust and bird droppings, achieving an accuracy of 91.46%, while incorporating data augmentation and oversampling strategies to address dataset limitations.

Owing to the rapid advancement and availability of computational resources, the adoption of deep learning architectures in solar PV analysis has become widespread. However, these methods still face critical challenges, including limited labeled data, class imbalance, low-contrast fault patterns, and high inter-class similarity. To address these issues, researchers have sought to improve existing models through architectural modifications, preprocessing techniques, and data augmentation strategies. Nevertheless, real-world applications demand lightweight and efficient architectures capable of handling class imbalance without introducing excessive computational complexity, highlighting the need for performance-enhancing yet resource-efficient design strategies.

Material and Method

The proposed framework follows a structured pipeline, including dataset preparation, preprocessing, and data augmentation. A lightweight SE-MobileNet with channel-wise attention is employed for PV panel fault detection to enhance feature representation. The model is evaluated in terms of detection accuracy, computational complexity, and inference efficiency, demonstrating its suitability for real-time and large-scale applications. Figure 1 presents the overall flowchart of the proposed PV panel fault detection and classification framework.

Dataset Description

The solar photovoltaic dataset [22] is a publicly available dataset comprising 875 RGB images collected under diverse conditions and categorized into six classes for classification task. Five classes correspond to specific fault types, namely bird droppings, dusty panels, physical damage, electrical damage, and snow-covered, while the remaining class represents healthy (clean) solar panels. The dataset makes direct analysis of solar panel surfaces feasible using image processing techniques for fault detection. Example samples from each class are shown in Figure 2. Although the dataset exhibits considerable diversity in fault types, a noticeable class imbalance exists among the categories. Table 1 provides a quantitative and qualitative overview of the dataset distribution.

Table 1. Quantitative and qualitative overview of each class

Class Name	Description	Samples
Bird Drop	Panels contaminated by bird droppings	207
Clean	Panels in perfect condition	193
Dusty	Panels contaminated with dust	190
Electrical Damage	Hot spot and electrical defects	103
Physical Damage	Cracks and broken glass	69
Snow Covered	Partially or fully covered with snow	123

PV Panel Image Preprocessing

In classification tasks, preprocessing plays a crucial role in ensuring reliable model performance [20]. Variations in image characteristics, such as resolution, contrast, and class imbalance, can adversely affect feature learning and limit the generalization capability of deep learning models. To ensure compatibility with the proposed model and pre-trained benchmark models, all input images were resized to fixed spatial dimensions. Specifically, PV images were resized to 224×224 for CNN-based models and 384×384 for ViT model. In resizing process, reflection (symmetric) padding was applied along the shorter dimension to preserve the aspect ratio and avoid geometric distortion. Subsequently, images were downsampled using bicubic interpolation. Furthermore, all images were converted to single precision and scaled to the [0,1] range to ensure consistency with ImageNet-based pre-training.

Data Augmentation

Due to the limited number of PV class samples, a data augmentation technique was applied to increase sample variation and overcome the relative inter-class differences. The data augmentation steps improve the model's ability to generalize, thereby enhancing its predictive score [2], [4], [23].

To address the class imbalance in the PV surface fault dataset, data augmentation was applied exclusively to the training set. Since the dataset contains uneven class distributions, with some PV fault categories being represented by substantially fewer samples, the underrepresented classes were augmented more extensively during training. Specifically, on-the-fly data augmentation was performed using random rotations (−15° to 15°), horizontal reflections, translations within ±10 pixels along both axes, and scaling in the range of 0.9–1.1. Vertical flipping was intentionally avoided to preserve the realistic structural orientation of PV panels. This strategy increased the effective diversity of minority-class samples and partially alleviated the adverse influence of class imbalance on the learning process. The validation and test sets were kept in their original, non-augmented form to ensure an unbiased and realistic evaluation of model generalization.

Figure 2. Example images from the PV panel fault detection dataset, showing representative samples for each fault category and the healthy (clean) class

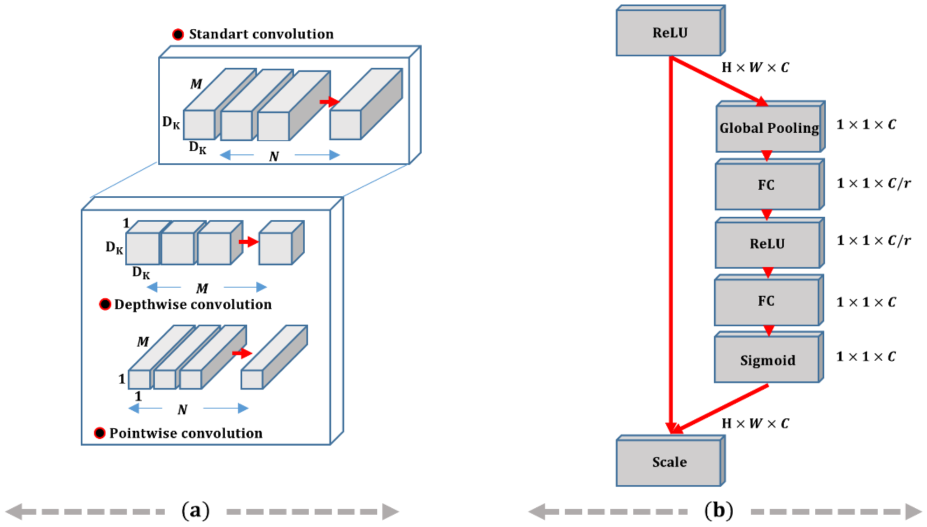

Figure 3. Core architectural components of the proposed model: (a) Depthwise separable convolution, (b) squeeze-and-excitation (SE) block for channel-wise feature recalibration.

SE-MobileNet

MobileNet [10] is a lightweight CNN architecture based on depthwise separable convolutions, primarily designed for embedded vision applications. Its efficient structure enables a balanced trade-off between computational cost and classification accuracy. Despite its lightweight design, MobileNet demonstrates competitive performance when compared to deeper and more complex architectures, making it a preferred choice for various image processing tasks [24], [25].

The MobileNet model relies on depthwise separable convolutions, which decompose standard convolutions into depthwise and 1x1 pointwise convolutions. This factorization significantly reduces computational cost and model size [10]. The computational cost for deep separable convolution and standard convolution is shown in Eqs. 1 and 2, respectively.

$$D_K^2 \cdot M \cdot D_F^2 + M \cdot N \cdot D_F^2 \qquad (1)$$

$$D_K^2 \cdot M \cdot N \cdot D_F^2 \qquad (2)$$

Here, The D_K denotes the spatial dimension of the square kernel, M and N represent the number of input and output channels, respectively. Similarly, D_F indicates the spatial dimension of the square input feature map. Consequently, depthwise separable convolution reduces the computational cost by around 8-9 times under typical settings. The depthwise separable convolution operation is illustrated in Figure 3 (a).

To improve model performance without compromising the computational efficiency of MobileNet, a Squeeze-and-Excitation (SE) block is integrated into the head of the network. The SE block [9] enhances channel-wise feature representation by explicitly modeling inter-channel dependencies. Specifically, global spatial information is first aggregated into a channel descriptor via a squeeze operation using global average pooling. For an input feature map $U \in R^{H \times W \times C}$, the channel-wise descriptor z_c is computed as:

$$z_c = \frac{1}{H \times W} \sum_{i=1}^{H} \sum_{j=1}^{W} U_c(i,j) \qquad (3)$$

where H, W, and C denote the height, width, and number of channels of the feature map, respectively. The excitation operation then learns channel-wise importance weights through two fully connected layers and non-linear activation functions:

$$s = \sigma\left(W_2 \delta(W_{1z})\right) \qquad (4)$$

where W_2 and W_1 are learnable parameters, δ denotes the ReLU activation function, and σ refers the sigmoid activation function. Finally, the input feature maps are recalibrated by multiplying each channel with its corresponding learned weight:

$$\breve{U} = s_c \cdot U_c \qquad (5)$$

Through this mechanism, the SE block emphasizes informative feature channels while suppressing less relevant ones. Notably, this enhancement is achieved with negligible additional computational overhead. The structure of the SE block is illustrated in Figure 3 (b).

Evaluation Metrics

To obtain robust and precise classification outcomes in photovoltaic fault detection, the selection of appropriate evaluation metrics is crucial. Due to the imbalance between classes, the chosen metrics should not negatively bias the performance assessment toward the majority class. In particular, precision, recall (sensitivity), and the F1-score (the harmonic mean of these metrics) are well-suited evaluation metrics [2]. In this study, the evaluation metrics used to distinguish between six different PV panel classes were computed on a per-class basis, including accuracy, sensitivity, specificity, precision, F1-score, and AUC. These metrics are defined in Eqs. (6)–(11).

$$accuracy = \frac{TP + TN}{TP + TN + FP + FN} \tag{6}$$

$$sensitivity = \frac{TP}{TP + FN} \tag{7}$$

$$specificity = \frac{TN}{TN + FP} \tag{8}$$

$$precision = \frac{TP}{TP + FP} \tag{9}$$

$$F1 - score = \frac{2TP}{2TP + FP + FN} \tag{10}$$

$$AUC = \int_0^1 TPR(FPR)d(FPR) \tag{11}$$

Here, TP, TN, FP, and FN denote true positive, true negative, false positive, and false negative, respectively. TPR and FPR represent the true positive rate and false positive rate, respectively.

Experimental Setup and Implementation Details

All experimental procedures were implemented in MATLAB 2025a (MathWorks, Natick, MA, USA) on a workstation configured with an NVIDIA RTX 5050 GPU (8 GB VRAM), 16 GB RAM, and an Intel i5-13450HX CPU.

For training the proposed model for PV fault classification, the RGB dataset was partitioned into training, validation, and test subsets with an approximate ratio of 0.6/0.2/0.2, respectively, within each fold. To ensure a reliable and fair evaluation of the generalization performance of both the proposed and benchmark models, a five-fold cross-validation-based evaluation procedure was performed. In this procedure, the training, validation, and test subsets were changed in each fold while preserving the same partitioning ratio. Therefore, the test set was not fixed or reused across all folds; instead, each fold included a different test subset. This approach enabled the models to be evaluated across diverse data splits rather than relying on a single fixed partition. The final performance values were reported as the mean and standard deviation of the metrics obtained over the five folds.

In classification tasks, the performance of deep learning models depends not only on architectural design but also on appropriate hyperparameter optimization during training [8]. During training, the proper selection of key hyperparameters, including the initial learning rate, optimization algorithm, batch size, and number of epochs, is critical for yielding stable convergence [23]. The MobileNet backbone was initialized with ImageNet-pretrained weights, while the newly added SE block and final classification layers were initialized from scratch. All layers were fine-tuned during training. Early stopping was monitored based on the validation loss with a patience value of 6. Specifically, training was stopped if the validation loss did not improve for six consecutive validation checks, and the network with the lowest validation loss was retained for final testing. The hyperparameter settings used in this study are summarized in Table 2.

Table 2. Summary of hyperparameter settings for the proposed and benchmark models.

Parameter	**Value**
Optimizer	Adam
Initial Learning Rate	1e-3
Learning Rate Schedule	Piecewise
Learn Rate Drop Factor	0.3
Learn Rate Drop Period	10 epochs
L2 Regularization	0.0005
Max Epochs	30
Mini-Batch Size	32
Shuffle	Every epoch
Validation Patience	6
Output Network	Best validation loss

Experimental Results

Performance Evaluation of the Proposed Model

After five-fold cross-validation, the model achieved robust classification performance on the test set. Overall, high accuracy values ranging from 0.914 to 0.974 and consistently high specificity values between 0.939 and 0.988 indicate reliable discrimination capability. In particular, the snow-covered class achieved the highest performance with an F1-score of 0.904, followed by electrical damage with an F1-score of 0.872. The proposed model achieved the best classification performance for the snow-covered class, with an F1-score of 0.904, followed by electrical damage with an F1-score of 0.872. However, the lowest performance was observed for the physical damage class, with an F1-score of 0.769.

Table 3. Class-wise mean (μ) and standard deviation (σ) of performance metrics for PV panel surface fault classification obtained by the lightweight channel attention-based network (MobileNet+SE) under five-fold cross-validation

Fault types	**Accuracy**		**Sensitivity**		**Specificity**		**Precision**		**F1-score**	
	μ	σ	μ	σ	μ	σ	μ	σ	μ	σ
Bird drop	0.933	0.020	0.860	0.050	0.956	0.014	0.856	0.044	0.858	0.044
Clean	0.914	0.018	0.824	0.108	0.939	0.024	0.795	0.046	0.805	0.049
Dusty	0.920	0.020	0.800	0.076	0.953	0.037	0.837	0.102	0.812	0.039
Electrical damage	0.969	0.021	0.893	0.087	0.980	0.015	0.855	0.100	0.872	0.085
Physical damage	0.966	0.010	0.754	0.164	0.984	0.007	0.804	0.060	0.769	0.093
Snow covered	0.974	0.010	0.887	0.059	0.988	0.010	0.926	0.056	0.904	0.039

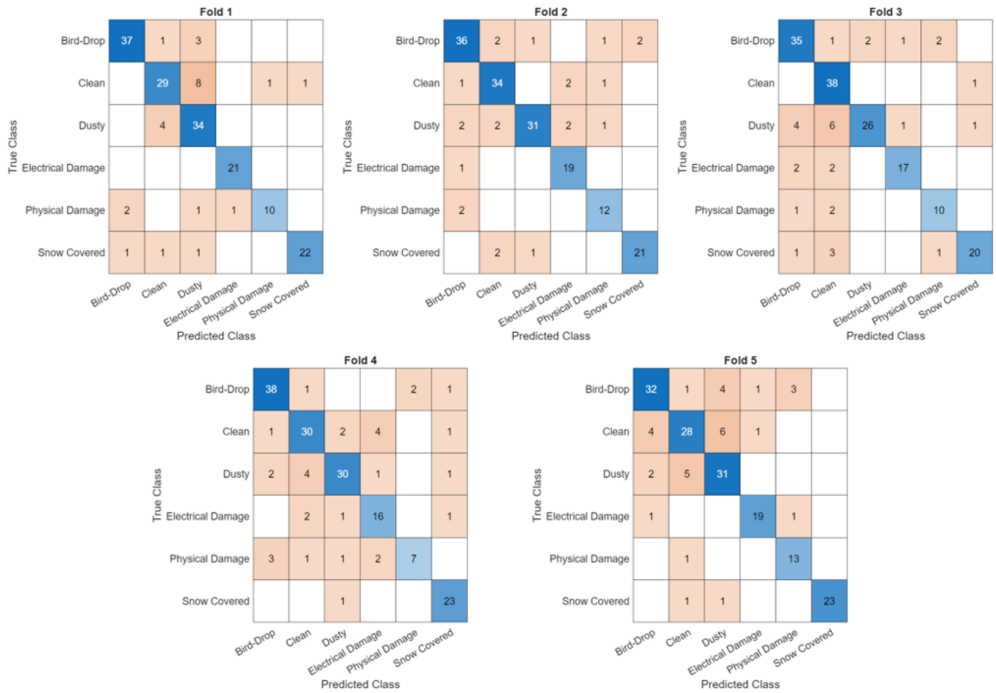

Figure 4. Fold-wise test confusion matrices obtained under five-fold cross-validation, with distinct test sample subsets used in each fold

From another perspective, relatively lower sensitivity values were observed for the physical damage (0.754) and dusty (0.800) classes, indicating that these categories are more challenging to detect, likely due to intra-class variability and visual similarity with other fault types. Despite this, the overall standard deviation values remained low across all metrics (generally ≤ 0.10), confirming the stability and consistency of the proposed model under different cross-validation folds. A detailed class-wise quantitative evaluation is provided in Table 3.

To complement the quantitative evaluation metrics, fold-specific confusion matrices are presented in Figure 4 illustrates the class-wise prediction distributions obtained across the five cross-validation folds. These matrices provide a detailed view of how the proposed model allocated predictions among the six fault categories and reveal the extent to which correct classifications concentrated along the principal diagonal.

As shown in Figure 4, the proposed lightweight fault classification model produced generally stable confusion patterns across the five folds. The electrical damage and snow-covered classes were classified with relatively high consistency, as most samples in these categories were correctly assigned to their true labels. In contrast, the highest classification ambiguity was observed between the clean and dusty classes. This confusion is reasonable because slight dust accumulation can cause only subtle visual differences in RGB images, making dusty panels visually similar to clean ones. Accordingly, several dusty samples were predicted as clean, and some clean samples were misclassified as dusty. Limited confusion was also observed between bird-drop and dusty classes, likely due to partially similar local contamination patterns on the panel surface. The physical damage class exhibited more fold-dependent variation, which may be associated with both the limited number of samples and the diverse visual appearance of physical defects. Overall, these results show that the model can effectively distinguish visually distinct PV fault categories, while subtle contamination-related classes remain more challenging.

To better illustrate the variability in classification performance across different data splits (training, validation, and test) for each class, boxplot distributions of the model performance obtained from different test samples under five-fold cross-validation are presented in Figure 5.

Among the classes, snow covered and electrical damage exhibit both high median values and relatively low variability, indicating robust and reliable classification. The clean class shows moderate performance with relatively stable distributions, although slightly lower median values are observed compared to other classes. Similarly, the dusty class presents moderate performance with remarkable variability, particularly in specificity and precision, suggesting challenges due to subtle visual differences and potential confusion with other classes. In contrast, physical damage shows the highest variability, especially in sensitivity and F1-score, indicating that it remains the most challenging class for consistent detection. Additionally, the consistently high AUC values across all classes confirm the strong discriminative capability of the proposed model. In Figure 6, the qualitative predictions of the proposed model for sample test images are demonstrated. These results indicate that the proposed model produces reliable confidence scores for real-world samples, demonstrating its robustness in practical scenarios

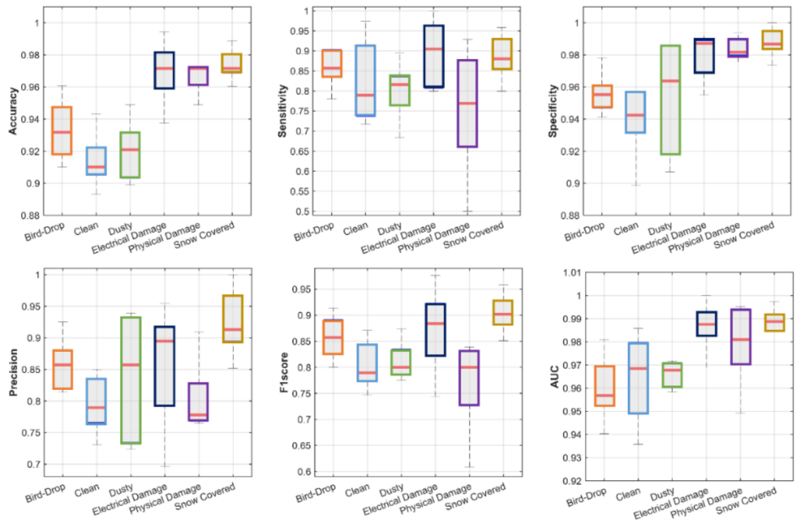

Figure 5. Box plot distributions of evaluation metrics across five-fold cross-validation.

Quantitative Comparison with Benchmark Models

To rigorously assess the effectiveness of the proposed model in PV fault diagnosis, a set of representative state-of-the-art architectures were systematically benchmarked under identical experimental settings. Specifically, the baseline MobileNet [10], DenseNet-201 [26], ResNet-50 [27], EfficientNet-B0 [28], and Vision Transformer (ViT) [29] models were employed for a comprehensive comparative evaluation. Table 4 demonstrates the class-wise comparative performance of the evaluated benchmark architectures for PV panel fault classification. The reported results represent the average performance metrics obtained after five-fold cross-validation. The proposed lightweight channel attention-based network achieved the highest accuracy in three of the six fault categories, reaching 0.933 for bird drop, 0.914 for clean, and 0.920 for dusty panel surfaces. For electrical damage faults and snow-covered samples, the proposed model yielded competitive accuracy at 0.969 and 0.974, closely approaching the highest values of 0.971 and 0.983 obtained by EfficientNetB0. For physical damage, the proposed model produced an accuracy of 0.966, matching DenseNet-201 and remaining close to the highest recorded value of 0.971.

Sensitivity performances further highlighted the class-wise detection capability of the proposed network. The highest sensitivity was obtained in bird drop classification with 0.860, exceeding DenseNet121 and EfficientNetB0 by 0.024 and 0.058, respectively. In dusty samples, sensitivity reached 0.800, representing the highest value among all tested models. For electrical damage, the proposed model achieved 0.893, matching the highest result observed in ResNet50. In snow-covered panels, sensitivity reached 0.887, slightly below the highest value of 0.919 reported by EfficientNetB0. Physical damage remained the most challenging class, where sensitivity reached 0.754, lower than EfficientNetB0 but higher than MobileNet baseline and ResNet50. On the other hand, specificity remained consistently high across all categories, with the proposed model reaching 0.956 in bird drop and 0.953 in dusty samples, both representing the highest specificity values within their respective classes.

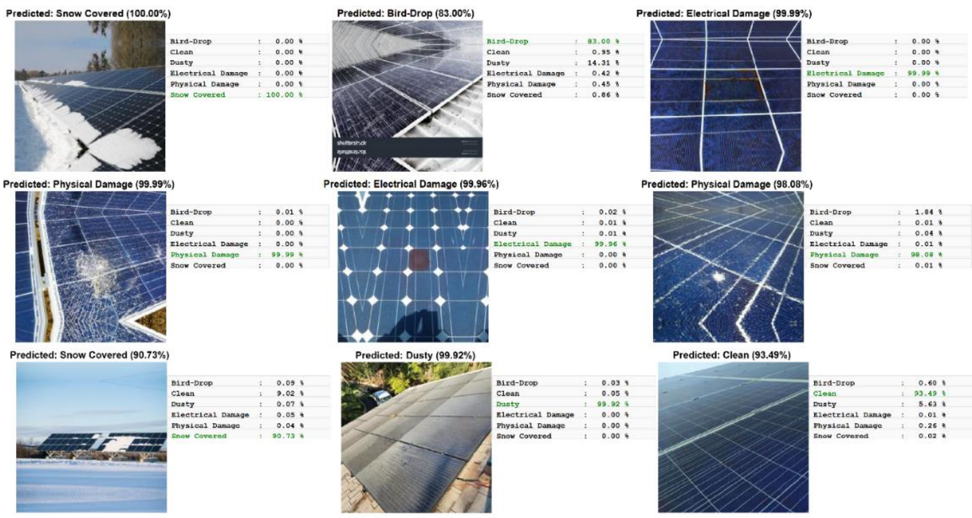

Figure 6. Qualitative results of the proposed model for PV panel fault classification. Each image is annotated with the predicted class label and corresponding confidence score.

Table 4. Overall comparative performance analysis of different CNN and transformer-based models for PV panel fault classification

	Faults types	DenseNet201	ResNet50	EfficientNetB0	ViT	MobileNet	SE-MobileNet
Accuracy	Bird drop	0.921	0.898	0.914	0.890	0.893	0.933
	Clean	0.909	0.904	0.916	0.899	0.901	0.914
	Dusty	0.907	0.910	0.904	0.876	0.894	0.920
	Electrical damage	0.974	0.967	0.971	0.963	0.967	0.969
	Physical damage	0.966	0.949	0.971	0.954	0.942	0.966
	Snow covered	0.973	0.963	0.983	0.950	0.960	0.974
Sensitivity	Bird drop	0.836	0.768	0.802	0.772	0.773	0.860
	Clean	0.856	0.830	0.850	0.751	0.850	0.824
	Dusty	0.758	0.758	0.758	0.679	0.689	0.800
	Electrical damage	0.883	0.893	0.874	0.884	0.882	0.893
	Physical damage	0.696	0.652	0.825	0.769	0.665	0.754
	Snow covered	0.886	0.844	0.919	0.812	0.790	0.887
Specificity	Bird drop	0.947	0.938	0.948	0.926	0.929	0.956
	Clean	0.923	0.925	0.935	0.941	0.915	0.939
	Dusty	0.948	0.951	0.944	0.930	0.950	0.953
	Electrical damage	0.986	0.977	0.983	0.973	0.978	0.980
	Physical damage	0.989	0.974	0.983	0.969	0.966	0.984
	Snow covered	0.987	0.982	0.993	0.972	0.988	0.988
Precision	Bird drop	0.830	0.801	0.837	0.790	0.772	0.856
	Clean	0.763	0.761	0.783	0.790	0.742	0.795
	Dusty	0.836	0.840	0.826	0.786	0.799	0.837
	Electrical damage	0.894	0.840	0.876	0.820	0.849	0.855
	Physical damage	0.843	0.683	0.820	0.718	0.658	0.804
	Snow covered	0.919	0.880	0.961	0.863	0.923	0.926
F1-score	Bird drop	0.832	0.779	0.812	0.769	0.771	0.858
	Clean	0.800	0.790	0.814	0.767	0.790	0.805
	Dusty	0.781	0.780	0.777	0.696	0.731	0.812
	Electrical damage	0.887	0.865	0.874	0.848	0.863	0.872
	Physical damage	0.758	0.665	0.815	0.729	0.654	0.769
	Snow covered	0.900	0.860	0.937	0.819	0.844	0.904
AUC	Bird drop	0.959	0.929	0.961	0.924	0.944	0.960
	Clean	0.963	0.948	0.967	0.946	0.946	0.964
	Dusty	0.957	0.951	0.951	0.953	0.947	0.966
	Electrical damage	0.989	0.979	0.992	0.977	0.987	0.987
	Physical damage	0.946	0.932	0.982	0.948	0.919	0.979
	Snow covered	0.993	0.987	0.997	0.990	0.971	0.989

Precision values obtained by the proposed model reached 0.856 in bird drop, 0.795 in clean surfaces, and 0.837 in dusty samples, corresponding to the highest precision values in these three categories. In physical damage, precision remained at 0.804, exceeding ResNet50, ViT, and baseline MobileNet, while snow-covered samples reached 0.926, remaining close to the highest value of 0.961 obtained by EfficientNetB0. Similar behavior was observed in F1-score values, where the proposed architecture achieved 0.858 in bird drop, 0.812 in dusty panels, and 0.904 in snow-covered samples, maintaining leading or near-leading performance in most classes.

To further validate the contribution of the proposed SE-based channel-wise feature recalibration mechanism, an additional paired statistical analysis was conducted using the fold-wise Macro F1 scores obtained from the five-fold cross-validation experiments. Macro F1 was selected as the reference metric because the dataset exhibits class imbalance, and this metric evaluates each class with equal importance regardless of class frequency. Therefore, it provides a more balanced assessment of the model's ability to distinguish different PV surface fault categories, particularly minority classes. Table 5 presents the fold-wise Macro F1 scores of MobileNet and SE-MobileNet, together with the paired statistical comparison results.

Table 5. Fold-wise Macro F1 scores and statistical comparison between MobileNet and SE-MobileNet

Fold/Statistic	MobileNet	SE-MobileNet	Difference
Fold 1	0.8464	0.8651	+0.0187
Fold 2	0.7563	0.8679	+0.1116
Fold 3	0.7077	0.8211	+0.1134
Fold 4	0.7721	0.7917	+0.0195
Fold 5	0.7951	0.8372	+0.0421
Mean ± SD	0.7755 ± 0.0510	0.8366 ± 0.0318	+0.0611 ± 0.0478
95% CI	-	-	[0.0016, 0.1205]
p-value	-	-	0.0463

As shown in Table 5, SE-MobileNet achieved higher Macro F1 scores than the baseline MobileNet in all folds. The mean Macro F1 score increased from 0.776 to 0.837, corresponding to a mean improvement of 0.0611. The paired t-test yielded a two-sided p-value of 0.0463, indicating that the improvement was statistically significant at the 0.05 level ($p < 0.05$). Moreover, the 95% confidence interval for the paired mean difference was [0.0016, 0.1205]. These findings statistically support the effectiveness of the proposed SE-based channel-wise feature recalibration mechanism in enhancing feature representation for PV surface fault classification.

In this study, the effect of data augmentation on the proposed model's performance was also investigated. For this purpose, the results obtained by SE-MobileNet with and without data augmentation were comparatively analyzed. Table 6 demonstrates the PV panel fault classification results of SE-MobileNet under both training settings. The reported values represent the average results obtained after five-fold cross-validation. Furthermore, the percentage performance improvement achieved with data augmentation compared with the non-augmented setting is also presented in Table 6.

As shown in Table 6, the application of data augmentation improved the overall classification performance of SE-MobileNet. The reported values represent the average results obtained after five-fold cross-validation. Sensitivity increased from 0.778 to 0.836, corresponding to a 7.46% improvement, while precision improved from 0.768 to 0.846, yielding a 10.11% increase. Similarly, the F1-score increased from 0.765 to 0.837, corresponding to a 9.41% improvement. In addition, accuracy, specificity, and AUC values also demonstrated performance improvements compared with the non-augmented training setting.

Complexity Analysis

In addition to classification accuracy, computational efficiency is critical for near real-time potential. Metrics such as inference time, FPS, and the number of model parameters play a key role in evaluating the practical applicability of deep learning models. Table 7 presents a comparison of the computational efficiency across all models.

The comparative complexity analysis demonstrates that the proposed SE-MobileNet model achieves a favorable trade-off between classification performance and computational efficiency. In terms of classification performance, the proposed model achieves a macro F1-score of 0.837 and a weighted F1-score of 0.838, which are among the highest across all benchmarking models.

From a computational efficiency perspective, SE-MobileNet achieves an inference time of 12.73 ms and a frame rate of 78.54 FPS, indicating efficient inference performance for visual applications. While EfficientNet-B0 provides comparable classification accuracy, it yields a significantly higher computational cost (37.50 ms inference time and 26.66 FPS), making it less suitable. Similarly, DenseNet121 and ViT exhibit substantially slower inference speeds (approximately 60 ms and 16 FPS) without providing a clear advantage in terms of F1-score.

Table 6. Effect of data augmentation on the performance of SE-MobileNet

Training Strategy	Accuracy	Sensitivity	Specificity	Precision	F1-score	AUC
Without data augmentation	0.923	0.778	0.953	0.768	0.765	0.954
With data augmentation	0.946	0.836	0.966	0.846	0.837	0.974
Improvement (%)	+2.49	+7.46	+1.36	+10.11	+9.41	+2.12

Table 7. Comparison of computational efficiency across all models

Model	Parameter size	Inference time (ms)	FPS	Macro F1-score	Weighted F1-score
Resnet50	23493766	10.75	92.96	0.789	0.794
MobileNet	2248614	12.08	82.80	0.776	0.779
Efficient-B0	4036242	37.50	26.66	0.838	0.830
DenseNet-121	18121478	61.70	16.21	0.826	0.824
ViT	57746694	60.70	16.48	0.771	0.766
SE-MobileNet	2625542	12.73	78.54	0.837	0.838

Discussion

In PV panel surface fault detection, the robustness of deep learning models should not be evaluated only based on their classification accuracy, but also in terms of their computational efficiency and suitability for practical deployment. In this regard, lightweight architectures play a critical role in enabling real-world applications. In this study, a lightweight convolutional neural network was adopted as the backbone and further enhanced with an effective channel attention mechanism to improve both detection and classification performance. The MobileNet architecture, which is specifically designed for embedded systems and offers a lightweight yet competitive classification performance, was selected as the backbone network. To further enhance channel-wise feature representation capability, the architecture was augmented with an SE block. The experimental results reveal that, while achieving a significant improvement in classification accuracy, the model renders no significant increase in computational cost. These results indicate that the proposed model achieves an effective trade-off between classification accuracy and computational efficiency.

In this study, rather than focusing solely on a binary classification task for PV panel fault detection, the emphasis is placed on distinguishing between different fault types. Different types of contamination can have varying impacts on PV power generation [1], [30]. In addition to surface contamination, electrical and physical faults may pose serious safety and irreversible risks [4]. Therefore, accurately and timely identifying and distinguishing fault types is of critical importance for reliable and safe PV system operation. The ability of the proposed model to accurately distinguish between six different fault types, while maintaining high inference speed (FPS), highlights the practical relevance and effectiveness of the proposed approach for real-world PV monitoring potentials.

RGB imaging provides a practical and cost-effective solution for detecting surface-level defects in PV panels, including dust deposition, bird droppings, and physical damage [18]. In recent years, RGB-based approaches have been widely adopted in PV fault detection studies, with several works utilizing the same benchmark dataset employed in this study [2], [18], [20], [21], [31], [32]. Although these studies report competitive class-level performance using state-of-the-art models, conducting a fair benchmark comparison remains challenging due to variations in experimental protocols, including data splitting strategies, cross-validation schemes, evaluation metrics, and data augmentation techniques.

In this context, the proposed SE-MobileNet model achieves macro and weighted F1-scores of 0.837 and 0.838, respectively, across six fault classes. These results indicate that the model provides a favorable balance between computational efficiency and classification performance. However, a direct and absolute performance comparison with existing studies may not be entirely appropriate due to the aforementioned methodological differences.

Conclusion

This study proposes a lightweight channel attention-based architecture for photovoltaic panel fault classification, built upon a MobileNet backbone to maintain computational efficiency. In order to enhance representational robustness without introducing significant overhead, a channel-wise attention mechanism is incorporated, enabling adaptive feature recalibration that prioritizes informative responses while suppressing less relevant ones.

The experimental findings indicate that this modification leads to a notable improvement in classification performance while maintaining high inference efficiency. In particular, the macro F1-score increases from 0.776 to 0.837, demonstrating the effectiveness of channel-wise refinement. These results demonstrate that the proposed design provides a favorable balance between accuracy and model complexity, highlighting its suitability for practical and real-time deployment scenarios.

In future work, the integration of multi-modal data is planned to improve diagnostic ability. Prior to the classification process, the semantic segmentation or bounding-box-based localization of defective regions on PV panels will be investigated to better distinguish contamination-related conditions, such as dust and bird droppings, from damage-related defects. This direction is expected to enable the proposed approach to extract more meaningful features directly from the regions of interest (RoI) rather than from the entire image. In addition to fault detection and classification, further efforts will focus on localizing the spatial distribution of faults on the panel surface and quantitatively estimating the associated power losses. Furthermore, the exploration of a lightweight hybrid framework that integrates segmentation and classification models is planned to improve both fault localization and diagnostic performance while maintaining computational efficiency.

Ethics committee approval and conflict of interest statement

This research was conducted without the need for ethics committee approval. No conflicts of interest are declared.

References

[1] S. Shaik *et al.*, "Experimental analysis on the impacts of soil deposition and bird droppings on the thermal performance of photovoltaic panels," *Case Stud. Therm. Eng.*, vol. 48, no. March, 2023, doi: 10.1016/j.csite.2023.103128.

[2] R. A. M. Rudro *et al.*, "SPF-Net: Solar panel fault detection using U-Net based deep learning image classification," *Energy Reports*, vol. 12, no. July, pp. 1580–1594, 2024, doi: 10.1016/j.egyr.2024.07.044.

[3] A. Sohail, N. Ul Islam, A. Ul Haq, S. Ul Islam, I. Shafi, and J. Park, "Fault detection and computation of power in PV cells under faulty conditions using deep-learning," *Energy Reports*, vol. 9, pp. 4325–4336, 2023, doi: 10.1016/j.egyr.2023.03.094.

[4] A. Rodrigo, I. Munasinghe, and A. Perera, "Vision-Based Object Detection for UAV Solar Panel Inspection Using an Enhanced Defects Dataset," 2025, [Online]. Available: http://arxiv.org/abs/2509.05348

[5] M. Jalal, I. U. Khalil, and A. ul Haq, "Deep learning approaches for visual faults diagnosis of photovoltaic systems: State-of-the-Art review," *Results Eng.*, vol. 23, no. July, p. 102622, 2024, doi: 10.1016/j.rineng.2024.102622.

[6] Y. Y. Hong and R. A. Pula, "Methods of photovoltaic fault detection and classification: A review," *Energy Reports*, vol. 8, pp. 5898–5929, 2022, doi: 10.1016/j.egyr.2022.04.043.

[7] K. Masita, A. Hasan, T. Shongwe, and H. A. Hilal, "Deep learning in defects detection of PV modules: A review," *Sol. Energy Adv.*, vol. 5, no. September 2024, p. 100090, 2025, doi: 10.1016/j.seja.2025.100090.

[8] M. N. Abuhashish, A. Refaat, A. Kalas, M. S. Hamad, and M. H. Elfar, "Towards accurate and reliable fault diagnosis in PV systems: Techniques, challenges, and future directions," *Process Saf. Environ. Prot.*, vol. 198, no. February, p. 107217, 2025, doi: 10.1016/j.psep.2025.107217.

[9] J. Hu, L. Shen, S. Albanie, G. Sun, and E. Wu, "Squeeze-and-Excitation Networks," *IEEE Trans. Pattern Anal. Mach. Intell.*, vol. 42, no. 8, pp. 2011–2023, 2020, doi: 10.1109/TPAMI.2019.2913372.

[10] A. G. Howard *et al.*, "MobileNets: Efficient Convolutional Neural Networks for Mobile Vision Applications," Apr. 2017, [Online]. Available: http://arxiv.org/abs/1704.04861

[11] R. Cavieres, R. Barraza, D. Estay, J. Bilbao, and P. Valdivia-Lefort, "Automatic soiling and partial shading assessment on PV modules through RGB images analysis," *Appl. Energy*, vol. 306, no. October 2021, 2022, doi: 10.1016/j.apenergy.2021.117964.

[12] K. Niazi, W. Akhtar, H. A. Khan, S. Sohaib, and A. K. Nasir, "Binary Classification of Defective Solar PV Modules Using Thermography," *2018 IEEE 7th World Conf. Photovolt. Energy Conversion, WCPEC 2018 - A Jt. Conf. 45th IEEE PVSC, 28th PVSEC 34th EU PVSEC*, no. 1, pp. 753–757, 2018, doi: 10.1109/PVSC.2018.8548138.

[13] A. Et-taleby, Y. Chaibi, N. Ayadi, B. Elkari, M. Benslimane, and Z. Chalh, "Enhancing fault detection and classification in photovoltaic systems based on a hybrid approach using fuzzy logic algorithm and thermal image processing," *Sci. African*, vol. 28, no. November 2024, p. e02684, 2025, doi: 10.1016/j.sciaf.2025.e02684.

[14] W. M. Shaban, "Detection and classification of photovoltaic module defects based on artificial intelligence," *Neural Comput. Appl.*, vol. 36, no. 27, pp. 16769–16796, 2024, doi: 10.1007/s00521-024-10000-z.

[15] M. U. Ali, H. F. Khan, M. Masud, K. D. Kallu, and A. Zafar, "A machine learning framework to identify the hotspot in photovoltaic module using infrared thermography," *Sol. Energy*, vol. 208, no. May, pp. 643–651, 2020, doi: 10.1016/j.solener.2020.08.027.

[16] D. Marletta, A. Midolo, and E. Tramontana, "Detecting Photovoltaic Panels in Aerial Images by Means of Characterising Colours," *Technologies*, vol. 11, no. 6, 2023, doi: 10.3390/technologies11060174.

[17] I. Ibn Malek and H. Imtiaz, "Advanced fault detection in PV panels using deep neural networks: leveraging transfer learning and electroluminescence image processing," *Energy Adv.*, pp. 180–193, 2025, doi: 10.1039/d5ya00239g.

[18] P. R. Sonawane, S. Bhandari, R. B. Patil, and S. Al-Dahidi, "Comparative analysis of methods used to solve class imbalance problem in dataset for CNN-based fault diagnosis of solar photovoltaic panels," *Int. J. Thermofluids*, vol. 28, no. June 2025, p. 101303, 2025, doi: 10.1016/j.ijft.2025.101303.

[19] R. Tang, Z. Ren, S. Ning, and Y. Zhang, "Fault classification of photovoltaic module infrared images based on transfer learning and interpretable convolutional neural network," *Sol. Energy*, vol. 276, no. March, p. 112703, 2024, doi: 10.1016/j.solener.2024.112703.

[20] O. F. Bamisile *et al.*, "Attention residual network with multi-scale convolution branch for efficient solar photovoltaic module defect classification," *Sol. Energy*, vol. 307, no. December 2025, p. 114323, 2026, doi: 10.1016/j.solener.2026.114323.

[21] Y. Ledmaoui, A. El Maghraoui, M. El Aroussi, and R. Saadane, "Enhanced Fault Detection in Photovoltaic Panels Using CNN-Based Classification with PyQt5 Implementation," *Sensors*, vol. 24, no. 22, pp. 1–20, 2024, doi: 10.3390/s24227407.

[22] "PV Panel Defect Dataset." Accessed: Apr. 07, 2026. [Online]. Available: https://www.kaggle.com/datasets/alicjalena/pv-panel-defect-dataset

[23] K. Awedat, G. Comert, M. Ayad, and A. Mrebit, "Advanced fault detection in photovoltaic panels using enhanced U-Net architectures," *Mach. Learn. with Appl.*, vol. 20, no. February, p. 100636, 2025, doi: 10.1016/j.mlwa.2025.100636.

[24] H. Polat, "Time-Frequency Complexity Maps for EEG-Based Diagnosis of Alzheimer ' s Disease Using a Lightweight Deep Neural Network Traitement du Signal Time-Frequency Complexity Maps for EEG- Based Diagnosis of Alzheimer ' s Disease Using a Lightweight Deep Neural N," no. December 2022, 2023, doi: 10.18280/ts.390623.

[25] H. Polat, "DAMMD-Net: A lightweight and enhanced deep segmentation network for skin lesion detection," *Digit. Signal Process. A Rev. J.*, vol. 167, no. 1, p. 105477, 2025, doi: 10.1016/j.dsp.2025.105477.

[26] G. Huang, Z. Liu, L. Van Der Maaten, and K. Q. Weinberger, "Densely connected convolutional networks," *Proc. - 30th IEEE Conf. Comput. Vis. Pattern Recognition, CVPR 2017*, vol. 2017-Janua, pp. 2261–2269, 2017, doi: 10.1109/CVPR.2017.243.

[27] K. He, X. Zhang, S. Ren, and J. Sun, "Deep residual learning for image recognition," *Proc. IEEE Comput. Soc. Conf. Comput. Vis. Pattern Recognit.*, vol. 2016-Decem, pp. 770–778, 2016, doi: 10.1109/CVPR.2016.90.

[28] M. Tan and Q. V. Le, "EfficientNet: Rethinking model scaling for convolutional neural networks," *36th Int. Conf. Mach. Learn. ICML 2019*, vol. 2019-June, pp. 10691–10700, 2019.

[29] A. Dosovitskiy *et al.*, "an Image Is Worth 16X16 Words: Transformers for Image Recognition At Scale," *ICLR 2021 - 9th Int. Conf. Learn. Represent.*, 2021.

[30] A. Khalifeh and R. Ghanem, "Solar Panel Soiling Classification Using Machine Learning Algorithms," *2024 25th Int. Arab Conf. Inf. Technol. ACIT 2024*, pp. 1–5, 2024, doi: 10.1109/ACIT62805.2024.10877104.

[31] M. R. Shoaib, H. M. Emara, J. Zhao, M. T. Ahvanooey, and E. Nabil, "Advanced deep learning approaches for fault detection in solar PV systems: A comparative study of SPDA and AIFD-SolDL," *Appl. Soft Comput.*, vol. 184, no. PB, p. 113592, 2025, doi: 10.1016/j.asoc.2025.113592.

[32] M. Eshwaran Ramachandran, G. Babu Balachandran, P. Velladurai, and A. Rajakumar, "Deep learning for solar PV fault classification using RGB imaging and comparison of preprocessing techniques," *Sol. Energy*, vol. 301, no. May, p. 113959, 2025, doi: 10.1016/j.solener.2025.113959.